LAWRENCE
LIVERMORE
NATIONAL
LABORATORY

LLNL-PROC-607292

Inverse Free Electron Laser Acceleration Using Ultra-Fast Solid State Laser Technology

S. G. Anderson, G. G. Anderson, S. M. Betts, S. E. Fisher, D. J. Gibson, A. M. Tremaine, S. S. Wu, J. T. Moody, P. Musumeci

December 7, 2012

International Particle Accelerator Conference
New Orleans, LA, United States
May 20, 2012 through May 25, 2012

Disclaimer

INVERSE FREE ELECTRON LASER ACCELERATION USING ULTRA-FAST SOLID STATE LASER TECHNOLOGY*

S.G. Anderson†, G.G. Anderson, S.M. Betts, S.E. Fisher, D.J. Gibson,
A.M. Tremaine, S.S. Wu, LLNL, Livermore, CA 94550, USA
J.T. Moody, P. Musumeci, UCLA, Los Angeles, CA 90095, USA

Abstract

We present a theoretical and computational study of the application of Ti:Sapphire laser technology to Inverse Free Electron Laser (IFEL) accelerators. Specifically, the regime in which the number of undulator periods is comparable to the number of cycles in the laser pulse is investigated and modifications to the IFEL accelerator equations and laser requirements are given. Simulations are used to study the IFEL interaction in this regime. In addition, the effects of non-Gaussian laser pulses are analyzed. Finally, the tools developed for this study are applied to the LLNL/UCLA IFEL experiment, and potential future IFEL designs.

INTRODUCTION

The IFEL acceleration mechanism was first proposed and analyzed in the 1980s [1, 2]. It is a promising candidate to demonstrate high gradient, high quality acceleration within the 50 MeV to few GeV energy range and is an attractive acceleration mechanism for compact light sources requiring moderate electron beam energies. In first generation experiments, researchers demonstrated the IFEL mechanism as an effective pre-buncher [3], high beam trapping — 85% [4], and high gradient — 70 MeV/m [5], but never simultaneously, and no post IFEL acceleration beam quality measurements have been performed.

The IFEL scheme considered here combines 800 nm, Ti:Sapphire laser technology with strongly tapered permanent magnet undulators. This enables a compact accelerator with increased beam energy and energy gain using the same undulator as the previous CO_2 laser-based experiment [5]. Concurrently, the repetition rate is increased by several orders of magnitude, allowing multi-shot emittance measurements to determine the quality of the accelerated beam.

The multi-TW peak laser power required for high accelerating gradient is accomplished by compression to subpicosecond pulse duration. In contrast to CO_2 laser experiments, these pulses can be short relative to the electron bunch duration and comparable to the amount of slippage in the undulator. We examine the consequences of using a short pulse laser to drive the IFEL in theoretical calculations and simulations. It is typical in Joule-class Ti:Sapphire lasers to produce a spatial profile that is somewhat more uniform than a Gaussian distribution due to gain saturation in the final amplifier. We simulate the potential degradation of IFEL performance due to this effect by using the "Flattened Gaussian" [6] formalism to propagate the laser through the IFEL interaction.

The simulation tools described below have been used to guide the choice of laser parameters [7], and model the expected performance of the LLNL/UCLA IFEL experiment [8]. Here we compare the effects of Gaussian and Flattened Gaussian laser profiles in this experiment and present a potential upgraded IFEL accelerator using a pre-buncher and optimized undulator design.

SHORT LASER PULSE EFFECTS

The original IFEL analysis performed in Ref. [2] derives equations for the evolution of particle energy, $\gamma = E/mc^2$, and phase, ψ, for an electron acted upon by a sinusoidal undulator magnetic field on the beam axis, and a plane electromagnetic wave. We consider instead a laser beam that is strongly focused (Rayleigh range much less than undulator length), and short duration (number of laser cycles and undulator periods is comparable). In the case of the LLNL/UCLA experiment there are 19 undulator periods and approximately 40 laser cycles in the pulse duration.

To rewrite the accelerator equations in this case, we assume a Gaussian spatial and temporal profile, giving the on-axis electric field,

$$\mathbf{E}_L = E_0 \mathrm{e}^{-\frac{(kz-\omega t)^2}{(\omega\tau)^2}} \frac{w_0}{w\left(z\right)} \cos\left(kz - \omega t - \phi_G\right) \hat{\mathbf{x}}, \quad (1)$$

where E_0 is the peak electric field, k the laser wave number, $\omega = ck$, 2τ the e^{-2} intensity pulse duration, $w_0/w\left(z\right)$ the ratio of the minimum beam size to that at position z, and ϕ_G is the Gouy phase. Using a planar undulator magnetic field and following the same analysis as Ref. [2], we find the accelerator equations,

$$\begin{aligned} \frac{d\gamma}{dz} &= \frac{1}{2}\frac{kK_L K_w}{\gamma}\mathrm{JJ}\sin\psi \\ \frac{d\psi}{dz} &= k_w \\ &\quad - k\frac{1 + K_w^2/2 + K_L^2/2 + K_w K_L \mathrm{JJ}\cos\psi}{2\gamma^2} \end{aligned} \quad (2)$$

*This work performed under the auspices of the U.S. Department of Energy by Lawrence Livermore National Laboratory under Contract DE-AC52-07NA27344.

† anderson131@llnl.gov

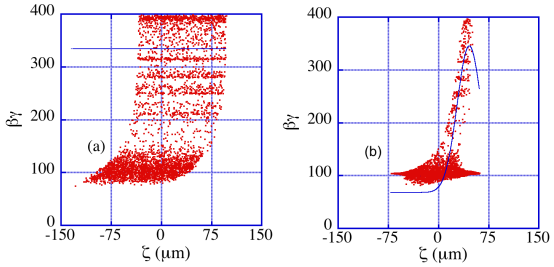

Figure 1: Longitudinal phase space exiting the undulator for (a) 3 TW long laser pulse and (b) 3 TW peak, 100 fs FWHM pulse. In each case the solid line depicts the longitudinal dependence of the laser field amplitude at the undulator exit.

$$-\frac{1}{z_r\left[1+\left(\frac{z}{z_r}\right)^2\right]}. \tag{3}$$

Here, $\psi = (k+k_w)z - \omega t - \phi_G$ is the relative phase, $K_w = \frac{eB_0}{mck_w}$ the normalized undulator strength and,

$$K_L = \frac{eE_0}{mc^2k}\frac{w_0}{w(z)}\mathrm{e}^{-\frac{(kz-\omega t)^2}{(\omega\tau)^2}} \tag{4}$$

is the normalized laser field strength. JJ is the usual Bessel function term arising in planar geometries, and $z_r = kw_0^2/2$ is the laser Rayleigh range.

Besides the modification to the phase evolution due to the Gouy phase shift [9], Eqns. 2 and 3 have a dependence of K_L on the global values of z and t. The laser vector potential used to derive these equations uses the Slowly Varying Envelope Approximation (SVEA), in this case that $\omega\tau \gg 1$ and $kz_r \gg 1$.

A simulation code has been developed to model the short pulse IFEL dynamics. In the simulation results that follow, particles are pushed using the Lorentz force law through the IFEL interaction using measured (or derived in the case of the proposed upgrade experiment) undulator field data, $\mathbf{B}_w$, and Gaussian or Flattened Gaussian laser pulses, which provide self-consistent phase and intensity evolution of the laser pulse.

In the simplest case, we examine the effect of a short laser pulse on the LLNL/UCLA experiment by comparing simulations of a 100 fs FWHM, 3 TW peak power laser, with a 3 TW laser with pulse length much longer that the interaction length in the 50 cm UCLA/Kurchatov undulator. For this comparison the injected electron beam is monoenergetic with particles equally spaced in phase. The simulated longitudinal phase space of the exiting beam is shown for both lasers in Fig. 1. In the long pulse case, each electron beam slice acts identically, as one expects, and we see a well defined captured bunch just below $\beta\gamma = 400$. In the short pulse case, the window of accelerated particles has approximately the same duration as the laser pulse, and there are very few particles captured that exit the accelerator at full energy. While 3 TW is sufficient laser power when applied through the entire interaction, it is insufficient when using 100 fs, FWHM pulses, since all beam slices are below the capture threshold for some part of the interaction. The result is that the peak laser power must be increased for short pulse IFEL to produce sufficient capture in the duration of the laser pulse. In the case of the present experiment, simulations indicated that at least 4-500 mJ of laser energy will be required [7].

FLATTENED GAUSSIANS

Use of a non-Gaussian laser spatial profile can degrade the IFEL performance due to reduced on-axis laser intensity given the same focusing parameters. This effect is expected in the LLNL/UCLA experiment based on the observed profile of the amplifier output beam. It is convenient to use the Flattened Gaussian Beam (FGB) formalism [6], where the laser field can be written as

$$U_N(r) = A_0\exp\left(-\frac{(N+1)\,r^2}{w_0^2}\right)\sum_{n=0}^{N}\frac{1}{n!}\left(\frac{(N+1)\,r^2}{w_0^2}\right), \tag{5}$$

where N is the integer order of the FGB greater than or equal to zero, A_0 is a normalization factor, and w_0 is a positive parameter. The field profile can be propagated analytically through paraxial symmetric optical systems as described in Ref. [6].

Figure 2 shows the spatial profile of 0^{th} (Gaussian), 4^{th}, and 8^{th} order FGBs at a focusing optic, the undulator entrance, and the center of the undulator for the LLNL/UCLA experiment. For each order, the intensity was normalized to give a total pulse energy of 550 mJ, and the same initial value of w_0 was used (consistent with the required 3.5 cm Rayleigh range at the undulator center). Start-to-end simulations of the LLNL/UCLA experiment are described in Ref. [8], and comparison runs were performed using the FGB laser profiles of Fig. 2. The resulting output momentum spectra using each FGB order are shown in Fig. 3. For 550 mJ, 100 fsec laser pulses, the figure shows that there is moderate decrease in the amount of beam captured and increase in the energy spread for the higher order FGBs. If these laser parameters are achieved in the experiment, the effect is expected to be manageable, as measured laser profiles from the amplifier are best fit using an FGB order between 2 and 4.

OPTIMIZED PLANAR UNDULATOR DESIGN

A number of upgrade options exist for future Ti:Sapphire IFEL projects at LLNL. These include the use of helical undulators and increased laser energy to produce GeV/m gradients and GeV output energies [10]. For Compton-scattering γ-ray source applications compact, several hundred MeV accelerators with low energy spread are desir-

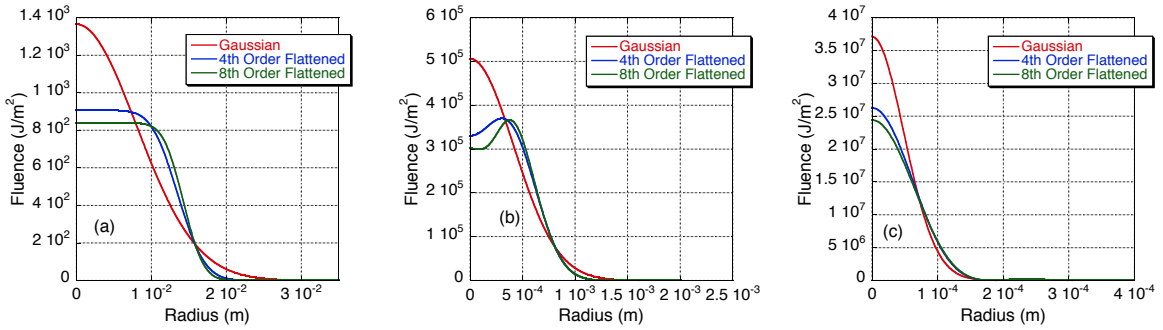

Figure 2: Flattened Gaussian intensity profiles simulated at (a) the IFEL final focus optic, (b) the undulator entrance, and (c) the undulator center. Each profile is normalized to have the same amount of energy.

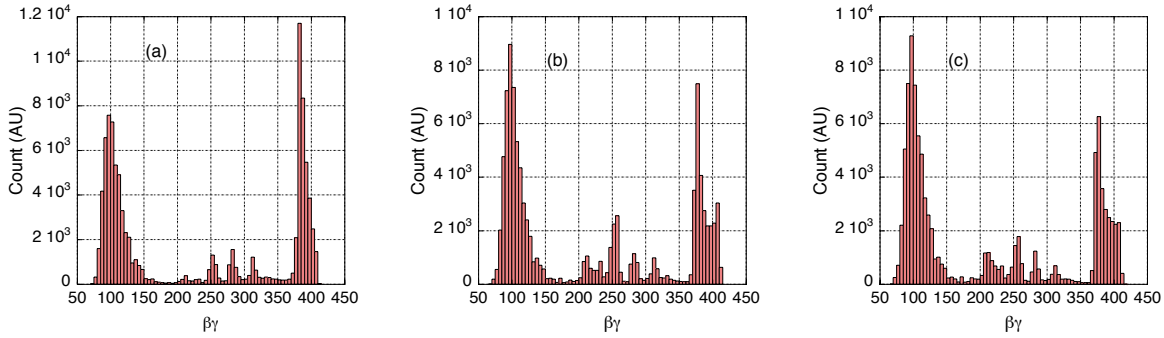

Figure 3: Simulated IFEL output momentum spectrum in the LLNL/UCLA experiment for (a) Gaussian, (b) 4^{th} order, and (c) 8^{th} order Flattened Gaussian laser profiles using 550 mJ and 100 fsec.

able. In this case, we are developing an IFEL design that uses the existing 500 mJ, 100 fsec laser in conjunction with a new planar undulator and pre-buncher.

In this design, the accelerator equations given above are used in the undulator optimization process described in Ref. [10] to determine the undulator field strength and period variation that optimally utilizes the available laser power. The theoretical undulator profile generated is shown in Fig. 4 and was imported into the IFEL simulation code to produce the output momentum spectrum shown. Here a 300 MeV electon beam is generated using a 50 MeV injector with 50% of the input beam captured, and an rms energy spread of 0.5%.

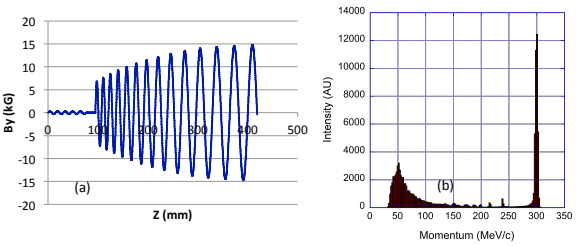

Figure 4: (a) Optimized planar undulator field design and (b) resulting IFEL momentum spectrum using the existing LLNL laser parameters.

REFERENCES

[1] R. Palmer, IEEE Trans. Nucl. Sci. **28** 3370 (1981).

[2] E.D. Courant, C. Pellegrini, and W. Zakowicz, Phys. Rev. A **32** 2813 (1985).

[3] Y. Liu, *et. al.*, Phys. Rev. Lett. **80** 4418 (1998).

[4] W.D. Kimura, *et. al.*, Phys. Rev. Lett. **86** 4041 (2001).

[5] P. Musumeci, *et. al.*, Phys. Rev. Lett. **94** 154801 (2005).

[6] M. Santarsiero, *et. al.*, Journal of Modern Optics, **44** p. 633 (1997).

[7] S.G. Anderson, *et. al.*, Proc. of PAC11, p. 331 (2011).

[8] J.T. Moody, *et. al.*, WEPPD053, these proceedings.

[9] P. Musumeci, Ph.D. Thesis, UCLA (2004).

[10] J.P. Duris, P. Musumeci, and R. K. Li, Accepted for Publication Phys. Rev. ST Accel. Beams (2012).